Environmental Science & Technology

pubs.acs.org/est

Article

# Sunlight Inactivation of Human Norovirus and Bacteriophage MS2 Using a Genome-Wide PCR-Based Approach and Enzyme Pretreatment

Stephanie K. Loeb, Wiley C. Jennings, Krista Rule Wigginton, and Alexandria B. Boehm*

Cite This: *Environ. Sci. Technol.* 2021, 55, 8783−8792

Read Online

ACCESS | Metrics & More | Article Recommendations | Supporting Information

**ABSTRACT:** Human norovirus (hNoV) is an important etiology of gastrointestinal illness and can be transmitted via ingestion of contaminated water. Currently impractical to culture, hNoV detection is reliant on real-time polymerase chain reaction (RT-PCR)-based methods. This approach cannot distinguish between infective and inactivated viruses because intact regions of the RNA genome can amplify even if the damage is present in other regions of the genome or because intact genetic material is not contained within an infectious virion. Herein, we employ a multiple long-amplicon RT-qPCR extrapolation approach to assay genome-wide damage and an enzymatic pretreatment to study the impact of simulated sunlight on the infectivity of hNoV in clear, sensitizer-free water. Using MS2 coliphage as an internal control, the genome-wide damage extrapolation approach, previously successfully applied for UV-254 inactivation, vastly overestimated sunlight inactivation, suggesting key differences in photoinactivation under different spectral conditions. hNoV genomic RNA was more susceptible to simulated sunlight degradation per base compared to MS2 genomic RNA, while enzymatic pretreatment indicated that hNoV experienced more capsid damage than MS2. This work provides practical and mechanistic insight into the endogenous sunlight inactivation of single-stranded RNA bacteriophage MS2, a widely used surrogate, and hNoV GII.4 Sydney, an important health-relevant virus, in clear sensitizer-free water.

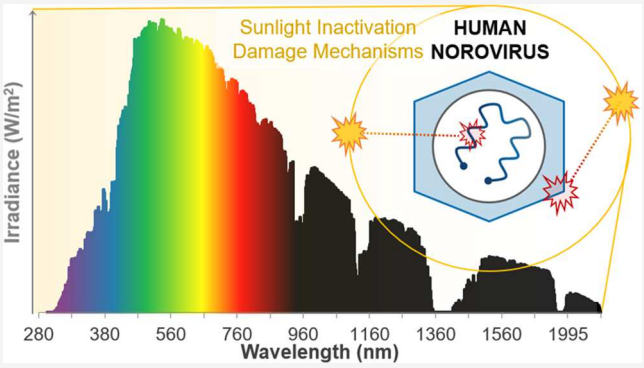


**KEYWORDS:** *norovirus, water, sunlight, photodamage mechanisms, photoinactivation, long amplicon, extrapolated RT-qPCR, capsid damage*



## INTRODUCTION

Globally, it is estimated that each year exposure to coastal waters polluted with wastewater causes an excess 120 million gastrointestinal and 50 million severe respiratory illnesses.[1] Evidence from saliva testing, epidemiology studies, and quantitative microbial risk assessments (QMRAs) suggests that human norovirus (hNoV) is the most important pathogen causing recreational waterborne illness.[2−5] Concurrently, hNoV has been detected in coastal waters globally.[6−9] Despite growing evidence of the importance of hNoV as a microbial pollutant in surface waters, there are very few studies examining its persistence, likely because it is extremely difficult to culture.[10,11] Previous research with indicators[12,13] or hNoV surrogate viruses[14−20] can provide a basis for understanding hNoV inactivation. However, these experiments have shown that specific differences in the genome sequence or the structure of capsid proteins can have large impacts on environmental persistence depending on the mechanism of inactivation. This emphasizes the need for research that directly studies hNoV.

The intensity and spectral shape of sunlight is a key factor influencing the rate of pathogen inactivation in the environment.[12,21−23] Photoinactivation can occur through the direct absorption of UV-B (280−320 nm) photons by components of the pathogen, such as nucleic acids, leading to the formation of deleterious photoproducts. Other chromophores within the pathogen can absorb longer wavelength visible and UV-A (320−390 nm) photons causing indirect damage through subsequent photosensitized oxidation reactions.[24,25] In viruses, photoinactivation typically relies on direct damage mechanisms as the simplistic structure of the virus lacks these photoreactive sensitizer components.[26−28] In some instances, photodamage can also occur through the photosensitization of molecules

Received: March 9, 2021
Revised: May 25, 2021
Accepted: May 26, 2021
Published: June 8, 2021

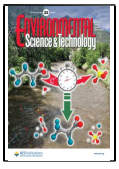

outside the virus, such as natural organic matter; however, many environmental conditions, including clear coastal waters,[13,29] are virtually free of external sensitizers. An understanding of the mechanisms of sunlight-induced photodamage is critical for predicting the persistence of pathogens in the environment.

The detection and quantification of hNoV in the environment has typically relied on molecular biology techniques, namely reverse transcription-quantitative polymerase chain reaction (RT-qPCR).[11,30] In a typical assay, a small (~60−200 bp (base pairs)) conserved region of the genome is selected for amplification. The rate of amplification is monitored and correlated with its initial concentration to infer the environmental concentration of hNoV. However, an intact region can amplify even if the damage is present in other regions of the genome or if intact genetic material is not contained within an infectious virion. This leads RT-qPCR to overestimate the number of infectious viruses in a sample[10,31] and underestimate viral inactivation rates.[32]

To address the latter shortcoming, a framework has been developed that uses RT-qPCR measurements to estimate the loss of infectivity for single-stranded RNA (ssRNA) viruses exposed to UV radiation. Assuming that UV photodamage is rare, random, and independent, this approach applies Poisson statistics to quantify genome-wide damage by extrapolating RT-qPCR results from several longer than typical amplicons across the entire genome.[33−37] If one photon damage event leads to an inactivated virus, i.e., the single-hit assumption, then the proportion of viruses that are infective can be determined by calculating the number of genomes with no damage sites defined by the no-hit probably in the Poisson distribution. Importantly, this approach permits an estimation of infectivity loss by assaying only a fraction of the genome, as directly measuring damage to the entire genome is impractical. However, due to heterogeneity in the response of individual amplicons, the accuracy of the approach increases as greater fractions of the genome are surveyed.[33,34] This genome-wide damage extrapolation has been successfully applied to predict the loss of infectivity for MS2[33] and hNoV[34] under UV-C (200−280 nm) light that is nearly monochromatic at 254 nm (UV-254), which is known to inactivate viruses via direct damage to the genome.[38,39] The applicability of this approach for predicting viral infectivity loss when exposed to broad-spectrum illumination, such as natural sunlight, has not yet been explored.

Considering approaches for assessing damage to non-genomic components of the virus, such as the capsid, enzymatic pretreatments have been used to distinguish between viable and inactivated viruses.[40−42] In this approach, a nuclease is applied to the sample prior to PCR amplification to degrade exposed genomic material with the aim of reducing detection of noninfectious viruses.[40−42] Previous work has shown that an RNase pretreatment prior to amplification, referred to as enzyme treatment RT-qPCR (ET-RT-qPCR), can prevent the amplification of RNA from noninfectious viruses inactivated by heat and chlorine treatments,[41,42] both thought to cause inactivation mainly through damage to capsid proteins.[43] In this work, we employ both the genome-wide damage extrapolation approach and an enzymatic pretreatment to study the impact of simulated sunlight on hNoV GII.4 Sydney and bacteriophage MS2 in clear, sensitizer-free water. The genogroup GII of hNoV is known to be responsible for the greatest number of norovirus illnesses in humans,[44] while the well-studied bacteriophage MS2 is used as an internal, biological control. By considering the extent of damage across the entire genome and the impact of damage to the capsid, this study provides important mechanistic insights into the environmental persistence of hNoV.

## MATERIALS AND METHODS

**Preparation of Virus Inoculants and Enumeration.** Lyophilized stocks of Enterobacteria phage MS2 DMS No. 13767 (MS2; GenBank accession number NC_001417; genome length 3569) and corresponding host *Escherichia coli* DMS No. 5695 (*E. coli*) were purchased from DSMZ German Collection of Microorganisms and Cell Cultures. Stocks were propagated according to manufacturer's specifications and maintained as glycerol stocks at −80 °C. MS2 inoculants for photoreactor experiments were prepared by processing a diluted aliquot of MS2 stock through a 100 kDa molecular weight cut-off Amicon Ultra membrane filter. The retentate was recovered by washing three times in phosphate buffer saline (PBS; VWR, pH 7.4). Purified inoculant was separated in 100 μL aliquots and stored at −80 °C until ready for use. MS2 concentrations were assayed using its *E. coli* host propagated in tryptic soy broth (TBS) with 2.0 mg/L streptomycin via a double agar soft-overlay technique as previously described.[45] Plates were incubated overnight at 37 °C, after which discretely formed viral plaques could be counted.

hNoV GII.4 Sydney (hNoV; GenBank accession number MK762570; genome length 7552) containing stool samples at a concentration of ~$10^8$ cp/mL were generously provided by Jan Vinje from the norovirus laboratory at the Centers for Disease Control and Prevention (CDC, Atlanta, GA). Stool samples were diluted 10X in PBS, vortexed thoroughly, and sonicated three times for 1 min each on ice to break-up aggregates.[46] Samples were then centrifuged at 4000*g* for 15 min to remove debris, and the virus-containing supernatant was reserved. The supernatant was diluted another 10X in sterile PBS and sequentially filtered through 0.8, 0.45, and 0.2 μm low-protein binding filters.[46,47] The filtered stool was processed through a 100 kDa molecular weight cut-off Amicon Ultra membrane filter, and the retentate was recovered by washing three times in PBS. Purified inoculant was separated in 200 μL aliquots and stored at −80 °C until ready for use.

**Sunlight Inactivation Experiments.** Experiments were performed in a Suntest CPS + solar simulator equipment with a circulating water bath. The water bath temperature was set to 15 °C and the Suntest irradiance was set to 250 W/$m^2$ (integrated intensity value over 300−800 nm, typical of morning sunlight on a clear day at a latitude of 40°N in the spring).[48] Irradiance values were externally verified by a SpectriLight ILT 950 fiber optic radiometer and SpectrILight III processing software. Schott WG280, WG305, and WG320 longpass 50% cut-off filters with 280, 305, and 320 nm cutoffs (Edmund Optics) were used to modulate the spectrum. For well-mixed collimated photoreactors, a depth average irradiance assuming that scattering and reflection loss at the surface are negligible is generally acceptable.[26] Spectra were measured through each optical filter, and the depth-averaged irradiance spectrum transmitted through the water column was calculated by correcting for light screening as previously described.[24,25] Experiments were conducted in batch reactors, consisting of glass beakers containing 9.7 mL of sterile PBS, covered with an optical filter and submerged in the water bath using flexible


https://doi.org/10.1021/acs.est.1c01575
Environ. Sci. Technol. 2021, 55, 8783−8792

wire flask weights. Dark controls were covered with aluminum foil. Purified inoculants were thawed on ice, and photoreactors were inoculated with 100 $\mu$L of MS2 and 200 $\mu$L of hNoV. Initial MS2 photoreactor concentrations ranged from $6.5 \times 10^6$ to $7.2 \times 10^5$ pfu/mL determined by plaque assay, and $2.5 \times 10^7$–$1.0 \times 10^8$ cp/mL as measured by RT-qPCR using the MP1 primer set (molecular methods to follow). Initial hNoV photoreactor concentrations ranged from $2.7 \times 10^6$ to $8.5 \times 10^5$ cp/mL as measured by RT-qPCR using the NR1 primer set (described below). Reactors were exposed to simulated solar light under continuous magnetic stirring for 8 h, removing 600 $\mu$L of sample aliquots each hour. The temperature was monitored throughout using an immersion thermometer placed in the water bath covered in foil adjacent to the photoreactor. Culture assays were performed on the same day, while two aliquots from each time point were stored at −80 °C for molecular analysis. A schematic diagram of the experimental workflow is shown in Figure S1.

UV–vis spectrophotometer (Uvikon XL Spectrophotometer, BioTek Instruments) analysis of photoreactor solutions containing purified MS2 and hNoV inoculants indicated a negligible difference in absorbance at relevant wavelengths (280–700 nm) compared to PBS alone, as shown in Figure S2. Although hNoV inoculants were thoroughly purified, the possibility that stool suspensions may contain reactive exogenous photosensitization compounds was further ruled out by comparing MS2 inactivation in PBS with and without the addition of hNoV (Figure S3).

**Enzymatic Pretreatment.** Prior to nucleic acid extraction, one aliquot from each time point was thawed and pretreated with RNase to neutralize exposed RNA present outside the capsid or inside damaged capsids.[41] Samples were treated with 0.1 U/$\mu$L RNase I at 37 °C for 15 min.[40,49] Nucleic acids were extracted from the samples immediately after treatment. Chemically induced RNase inactivation occurs implicitly during the initial steps of the nucleic extraction protocol,[50] obviating the need for an RNase inactivation step.

**Molecular Methods.** Nucleic acids were extracted using All Prep PowerViral DNA/RNA Kits (Qiagen) following manufacturer instructions for processing liquid samples without bead beating. An initial sample volume of 200 $\mu$L was eluted into 60 $\mu$L RNase-free water. cDNA synthesis was performed immediately after extraction, using the iScript cDNA synthesis kit (BioRad) with 15 $\mu$L template per reaction following the manufacturer's recommended protocol. Reactions were performed in triplicate, pooled, aliquoted, and stored at −80 °C until qPCR. An extraction blank containing 200 $\mu$L molecular grade water was included in each batch (approximately every 19 samples).

Ten candidate long-amplicon (~500 bp; 6.5% of the genome per amplicon) hNoV primer sets targeting non-overlapping regions of the genome were developed using Geneious bioinformatics and primer design software (version 11.1.5, Biomatters Ltd.). To validate primer set performance, aliquots of hNoV inoculant were extracted and amplified, and the PCR product was visualized on a 1.5% agarose gel in 1X TAE for 60 min at 100 V (Figure S4). cDNA standards for each amplicon were developed by excising the bands, processing with a QIAquick Gel Extraction Kit (Qiagen) and determining the product concentration using a Qubit fluorometer dsDNA kit (Invitrogen). Standards were diluted, aliquoted at a concentration of $10^6$ cp/2 $\mu$L, and stored at −80 °C. Immediately prior to use, standards were thawed and diluted into a 10X standard series. Assay performance was assessed by running a standard series from $1 \times 10^1$ to $1 \times 10^6$ cp/rxn using SYBR chemistry and analyzing both experimental and *in silico* melt curves (with uMelt[51]). Based on the reaction efficiency, sensitivity, and $R^2$, regions NR1 (norovirus region 1), NR2, NR6, and NR9 were selected and subsequently used to analyze samples from the photoinactivation experiments. Together, these four amplicons cover 1991 bases, representing 26% of the hNoV genome.

Twelve long-amplicon (~300 bp; 8% of the genome) assays for MS2 previously developed by Pecson et al.[42] were screened as described above for the hNoV candidates. Standards were prepared in the same manner as described for hNoV, by extracting and amplifying an aliquot of the purified MS2 inoculant. PCR products were visualized (Figure S5), and the bands were excised and used to produce cDNA standards. Regions MP1 (MS2 Pecson region 1), MP5, MP6, and MP8 were selected for use in the photoreactor experiments. Together, these four MS2 amplicons cover 1212 bases, representing 34% of the MS2 genome. Table S1 summarizes the performance of all candidate assays for MS2 and hNoV. The fractional base content for each assayed amplicon is shown in Figure S6.

For both hNoV and MS2, SYBR-based qPCR assays were performed in a 20 $\mu$L reaction containing 2 $\mu$L of cDNA template, 1X Fast Eva Green Master Mix (Biotium), 1X ROX passive reference dye, 0.5 $\mu$M of each primer, 0.625 mg/mL molecular grade bovine serum albumin, and molecular grade water with a fluorescence threshold of 0.02 ΔRn units. Concentrations were determined using plate-specific standard curves run in duplicate, along with duplicate no-template controls (NTCs) for each plate (Figure S7).

**Data Analysis.** First-order observed inactivation rate constants ($k$, cm$^2$/kJ, $\lambda$ = 280–700 nm) were calculated as the negative slope of the linear regression trend of $\ln(N(t)/N_0)$ versus the depth-averaged fluence transmitted through the water column integrated across a spectral range of 280–700 nm. $N_0$ and $N(t)$ are the initial and at time $t$ viable virus populations determined by plaque assay (pfu/mL). Likewise, degradation rate constants for individual amplicons were calculated as the negative slope of $\ln(x(t)/x_o)$ versus fluence, where $x_o$ and $x(t)$ are the initial and at time $t$ number of intact amplicons determined by RT-qPCR (copy (cp)/mL). $k$ values and their error were determined using the average and standard deviation of concentrations ($N$ and $x$) from duplicate experiments. When combining rate constants $k$ from multiple amplicons, the error was defined as the standard deviation between trials and the errors were propagated using standard propagation equations for normally distributed errors.

Photodamage to individual amplicons was extrapolated to estimate genome-wide damage by combining the RT-qPCR amplification results from four long-amplicon assays assuming that photon-induced damage follows a Poisson distribution. The proportion of fully intact genomes can be predicted by combining results from several amplicons as follows, where $N_0$ and $N$ are the concentrations of intact genomes before and after treatment (i.e., exposure to simulated sunlight), and the probability of finding an intact amplicon $i$ after a giving exposure time is $\frac{x_i}{x_{o,i}}$ for $n$ amplicons

$$\frac{N}{N_0} = \left[\prod_{i=1}^{n} \frac{x_i}{x_{o,i}}\right]^{\text{genome length/total length of } n \text{ amplicons}} \quad (1)$$



https://doi.org/10.1021/acs.est.1c01575
Environ. Sci. Technol. 2021, 55, 8783–8792

The genome-wide damage extrapolation and statistical analyses were performed in RStudio Version 1.2.1335. To compare $k$ values between conditions, an analysis of covariance was performed using a dummy variable to code for the categorical factor. Regressions of $\ln(N(t)/N_0)$ or $\ln(x(t)/x_o)$ versus fluence were allowed to interact with the dummy variable and interactions with a $p$-value < 0.05 were considered to have statistically significantly different rate constants. Sequence queries, including counts of paired pyrimidines bases, were determined using the BiocManager R package.[52] Fractional content for both single (U) and paired pyrimidine bases (CC, UU, and CU or UC) was calculated by dividing the count of occurrence by the total number of base pairs in the amplicon.

## RESULTS

**Solar Simulator Experimental Conditions.** The simulated solar spectrum used in this study compared to the American Society for Testing and Materials Terrestrial Reference Spectra air mass 1.5 (NREL AM1.5G),[53] a typical spectrum for mid-latitude US (40°N) ground level sunlight, is shown in Figure 1. Irradiance was measured using a spectroradiometer, which is preferred over actinometry when accuracy in the UV range is critical, as most chemical actinometers have an absorption spectrum largely different than the action spectrum important for photoinactivation.[26] The spectrum most closely approximates sunlight in the photobiologically relevant UV-B to blue regions, with deviations typical of xenon lamp spectra at wavelengths longer than 400 nm. A small amount of UV-C light was detected in the spectrum through the atmospheric filter alone; consequently, a 280 nm 50% longpass cut-off filter was used to refine the full spectrum condition. Subsequent 305 and 320 nm longpass filters were used to remove sequentially larger fractions of the UV-B region. Under full spectrum conditions (280 nm longpass filter), the spectrum contained 0.47% UV-B and 7.9% UV-A light, as a fraction of total energy integrated from 280 to 700 nm. Similarly, the fractional UV content was 0.36% UV-B and 7.8% UV-A for the 305 nm longpass filter condition, and 0.22% UV-B and 7.6% UV-A for the 320 nm longpass filter condition.

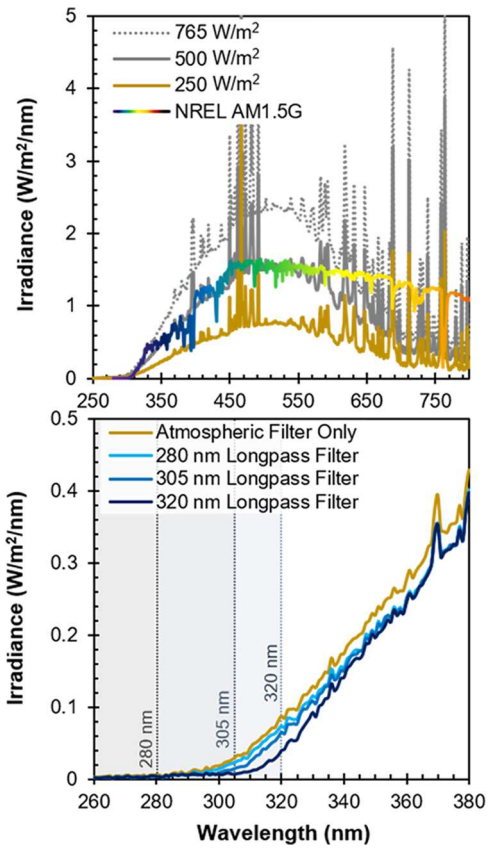


**Figure 1.** (Top) Solar simulator spectrum with different intensity settings overlaid with the American Society for Testing and Materials Terrestrial Reference Spectra for Photovoltaic Performance Evaluation reference air mass 1.5 spectra (NREL AM1.5G)[53] for comparison. (Bottom) Solar simulator output using the 50% cut-off longpass filters employed in this study for the most photobiologically relevant UV-B to blue light wavelengths.

Inactivation experiments were performed at an intensity setting of 250 W/m$^2$ to maintain consistently low-solution temperatures throughout the 8 h exposure time. Preliminary experiments indicated that higher intensity values could lead to elevated solution temperatures (Figure S8). With intensity values ~250 W/m$^2$, water temperatures were maintained below 25 °C and no dark inactivation was observed.

**Inactivation Kinetics.** Inactivation rate constants $k$ for MS2 measured using a plaque assay (culture-based assay) and for MS2 and hNoV measured using RT-qPCR signal loss are provided in Table 1, while linearized curves for each condition are shown in Figure 2. Degradation rate constants between various MS2 and hNoV amplicons were similar (Figures S9 and S10). MS2 bacteriophage was selected as an internal control because it is one of the most well-studied ssRNA viruses. Additionally, MS2 is particularly sensitive to inactivation via exogeneous photosensitization,[29] which allows us to confidently rule out the presence of exogenous photosensitizers in our purified inoculant, as the rate of MS2 inactivation did not increase in the presence of hNoV (Figure S3). All $k$ values were essentially 0 for all targets under dark conditions indicating that any observed decay under sunlit conditions can be attributed to photoinactivation.

We observed differences in $k$ values depending on the properties of the incident light among the three different virus-enumeration method conditions. For hNoV (by RT-qPCR) or MS2 using the culture assay ($p$ < 0.05), $k$ values measured under each spectral condition were significantly different with larger $k$ values for conditions with shorter wavelengths present. For MS2 measured by RT-qPCR, photodegradation was only observed when using the 280 and 305 nm cut-off filters, with these two experiments yielding similar $k$ values, $p$ = 0.49. Experiments using the 320 nm cut-off filter yielded a $k$ value not significantly different from that obtained under the dark condition ($p$ = 0.37). MS2 inactivation measured using a plaque assay resulted in significantly larger $k$ values for all light conditions compared to MS2 amplicon degradation measured via RT-qPCR. The RT-qPCR measured $k$ values were significantly larger for hNoV amplicons compared to MS2 amplicons for the full spectrum 280 nm cut-off filter condition and the 320 nm cut-off filter condition, but they were not different under 305 nm cut-off condition.

**Genome-Wide Damage Extrapolation.** For both MS2 and hNoV, RT-qPCR results for all four amplicons were combined using the genome-wide damage extrapolation described in eq 1 to estimate the proportion of fully intact genomes remaining at each time point (Table 1). An


https://doi.org/10.1021/acs.est.1c01575
Environ. Sci. Technol. 2021, 55, 8783−8792

**Table 1. Comparison of First-Order Rate Law $k$ ($cm^2/kJ$, $\lambda$ = 280−700 nm) for MS2 and hNoV GII.4 Determined Using the Cultured-Based Plaque Assay Method (MS2 only), RT-qPCR Signal-Loss (Average of Four Amplicons), Genome-Wide Damage Extrapolated Using eq 1, and Signal Loss from RT-qPCR with an RNase Pretreatment (ET-RT-qPCR)[a]**

| | First-order rate law $k$ ($cm^2/kJ$, $\lambda$ = 280−700 nm) | | | |
|---|---|---|---|---|
| | culture | RT-qPCR | extrapolated RT-qPCR | ET-RT-qPCR |
| | | **280 nm Longpass Filter** | | |
| MS2 | 7.3 ± 0.12 | 1.7 ± 0.20 | 20 ± 0.84 | 2.1 ± 0.14 |
| hNoV GII.4 | - | 4.2 ± 0.14 | 63 ± 0.46 | 5.6 ± 0.11 |
| | | **305 nm Longpass Filter** | | |
| MS2 | 3.7 ± 0.25 | 1.3 ± 0.32 | 16 ± 1.5 | 1.6 ± 0.24 |
| hNoV GII.4 | - | 2.7 ± 0.20 | 41 ± 1.3 | 4.0 ± 0.09 |
| | | **320 nm Longpass Filter** | | |
| MS2 | 2.1 ± 0.65 | −0.098 ± 0.26[b] | - | 0.29 ± 0.35[b] |
| hNoV GII.4 | - | 0.89 ± 0.24 | 13 ± 1.9 | 1.3 ± 0.27 |

[a]Experiments were performed in duplicate and error values are the propagated standard deviation between the two trails. A "-" indicates that the $k$ value was not measured. [b]Not significantly different from dark condition.

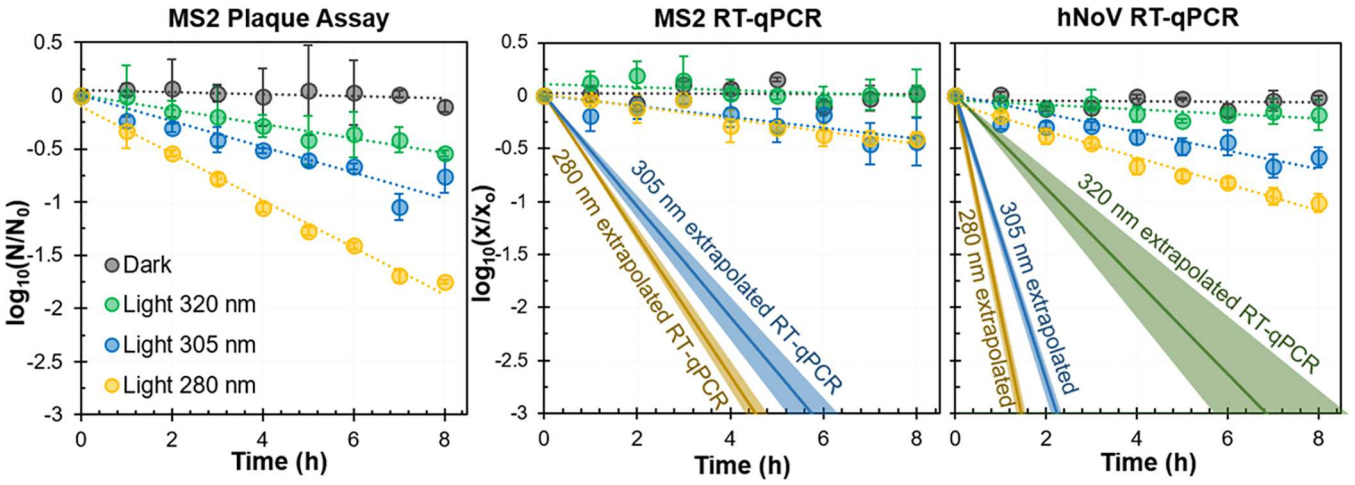


**Figure 2.** Inactivation kinetics for MS2 and hNoV with each longpass cut-off filter and in the dark. MS2 was measured using both a plaque assay (left) and RT-qPCR signal loss (center). hNoV was measured using RT-qPCR signal loss (right). For RT-qPCR measurements, amplicon degradation is displayed as an averaged result of all four amplicons to facilitate data visualization. Errors bars represent the standard deviation of two trials. For RT-qPCR data, genomic-wide damage was estimated by combining the RT-qPCR signal from four amplicons using the genome-wide damage extrapolation described in eq 1 and assuming that a single-damage site will render the virus inactive (single-hit assumption). The shaded area represents the propagated error for the extrapolation. No extrapolation was carried out on MS2 under 320 nm condition since no decay of amplicons was observed under this condition.

extrapolation was not performed for MS2 under the 320 nm cut-off filter condition as the rate constants for amplicon degradation were not significantly different from the dark condition. The resultant extrapolated kinetics are shown as solid lines in Figure 2 with a shaded region representing the standard deviation propagated through for the extrapolation calculation. Comparing the MS2 culture assay rate constant with the extrapolated $k$ value, the genome-wide damage extrapolation greatly overestimates the loss of MS2 infectivity. For the 280 nm spectral condition, the genome-wide damage extrapolation overestimated loss of infectivity by a factor of 2.7X compared to the plaque assay and overestimated infectivity by a factor of 4.3X for the 305 nm spectral condition. The extrapolated $k$ values for hNoV were significantly larger than the extrapolated MS2 rate constants under all light conditions. An analogous table with rate constants normalized by the total combined UV-B and UV-A doses (i.e., $\lambda$ = 280−390 nm) is provided in Table S2.

**Variation between Amplicons.** The degradation rate constants were similar between amplicons for the same virus, but $k$ values for hNoV amplicons were significantly larger than for MS2 amplicons (Figures S11 and S12). Since hNoV amplicons were ∼200 bp longer than MS2 amplicons, degradation rate constants for each individual amplicon were normalized by the number of bases and expressed as a function of the dose of simulated solar light energy integrated from 200 to 700 nm (Figure 3). Within each spectral condition, the $k$ values for individual amplicons of the same virus were not found to be statistically significantly different from each other. Although differences in the photodegradation rate between amplicons for the same virus were small, their relative $k$ values were generally consistent between trials and spectral conditions, e.g., amplicon MP6 exhibits the fastest degradation rate under all spectral conditions. When normalized by the number of bases, the loss of RT-qPCR signal remained statistically significantly higher for hNoV amplicons compared to MS2 amplicons for the 280 and 320 nm cut-off filter condition and not significant for the 305 nm cut-off filter condition ($p$ = 0.296). For the 280 nm condition, hNoV amplicon degradation rates were on average 47% larger than


https://doi.org/10.1021/acs.est.1c01575
Environ. Sci. Technol. 2021, 55, 8783−8792

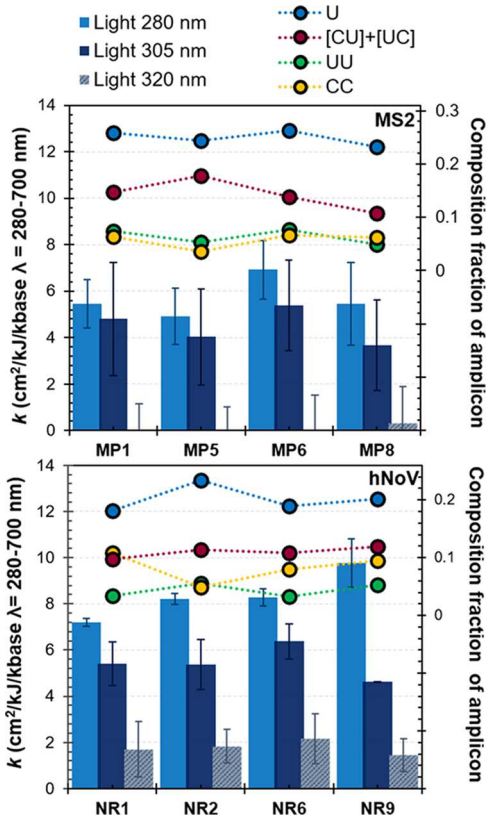


**Figure 3.** First-order degradation rate constants for each amplicon, under each light filter condition, normalized by the number of bases in the amplicon (shown as bars). Rate constants are compared with the fractional base content of selected nucleic acids for each amplicon (shown as filled circles). Fractional content for both single (U) and pyrimidine bases with an adjacent pyrimidine base (CC, UU, and CU or UC) was calculated by dividing the count of occurrence by the total number of bases in the amplicon. Rate constants were determined using standard first-order kinetic rate law $\ln\left(\frac{x}{x_o}\right) = -k \cdot I \cdot t$, where $I$ (W/m$^2$) is the integrated intensity from $\lambda$ = 280 to 700 nm and then dividing by the number of bases in the amplicon.

MS2 amplicon degradation rates (compared to 1.5× higher prior to normalized by the number of bases).

Variations in the nucleic acid sequence between amplicons are displayed as associated line graphs in Figure 3. Fractional content of adjacent pyrimidine bases UU, CC, or [CU] + [UC] as well as the total content of U bases was considered as a review of the literature indicated that pyrimidine dimers and possibly the formation of uridine hydrates may be the primary photoproducts driving inactivation with wavelengths in the UV-A and UV-B regions.[39,54−56] There was no evidence that amplicon-specific $k$ values were related to the fractional composition of adjacent pyrimidine bases. For MS2, the relative degradation rate between amplicons did visually appear to be positively correlated with an increase in uracil content; however, likely due to the similarity in $k$ values between amplicons and the overall small differences in uracil content between amplicons, this trend was found to be not statistically significant. With amplicon lengths over 300 bps, the differences in uracil content between MS2 amplicons ranged only from 23.1% for MP8 to 26.6% for MP6.

**Effect of Enzyme Treatment.** ET-RT-qPCR amplicon degradation rate constants were larger than the nontreatment case for all illumination conditions (Table 1 and linearized RT-qPCR signal-loss curves in Figure 4). However, the difference

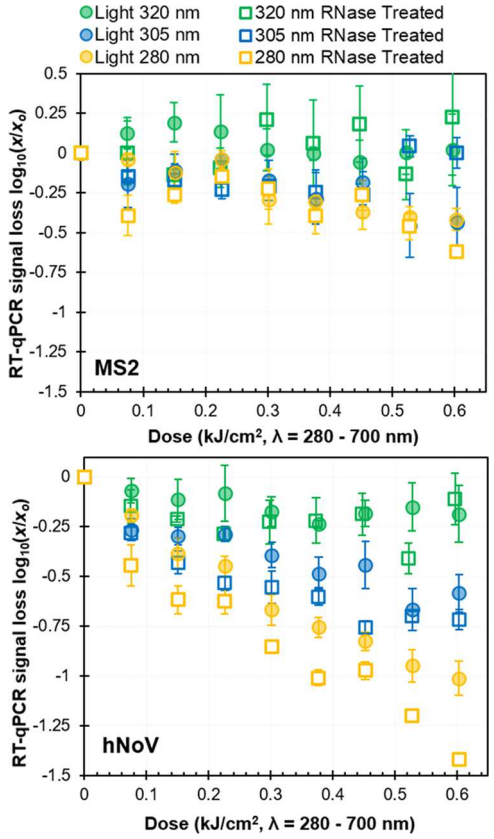


**Figure 4.** Loss of RT-qPCR signal for MS2 (top) and hNoV (bottom) grouped by light filter condition and enzymatic treatment. Filled circles represent the nontreatment condition, while open squares represent the associated RNase-treated sample for each time point. To aid visualization, amplicon degradation is presented as an averaged result for all four amplicons. Error bars represent the standard deviation of two trials propagated across the four amplicons.

was not significant for hNoV with the 320 nm cut-off filter or for MS2 under any spectral condition tested. The difference between the enzyme and nonenzyme treatment was statistically significant for hNoV amplicons under the 280 and 305 nm filter conditions. Using the ET-RT-qPCR method did not provide a drastic increase in $k$ values, with the enzyme treatment resulting in less than a 2-fold increase compared to the rate constants determined by RT-qPCR alone. Cases where the RNase treatment and nontreatment cases were not significantly different tended to show the least degradation over the 8 h time period.

For both the 280 and 305 nm filter conditions, the percent increase in rate constant between the enzyme treatment and nontreatment condition was significantly greater for hNoV than for MS2. For hNoV under the 280 nm filter condition, the ET-RT-qPCR rate constant was 33% larger than the RT-qPCR rate constant, whereas for MS2 under the 280 nm filter condition, the ET-RT-qPCR rate constant was 24% larger than the RT-qPCR rate constant.

Although amplicon degradation rate constants were larger measured by ET-RT-qPCR compared to RT-qPCR, they were


https://doi.org/10.1021/acs.est.1c01575
Environ. Sci. Technol. 2021, 55, 8783−8792

significantly smaller than the $k$ values measured for MS2 inactivation using the culture-based assay. For MS2 under the 280 nm filter condition, the culture-based rate constant was over 300% larger than the RT-qPCR rate constant, and nearly 250% larger than the ET-RT-qPCR rate constant.

## DISCUSSION

For each molecular method used to assay photodamage in this study (RT-qPCR, extrapolated RT-qPCR, and ET-RT-qPCR), hNoV appears to be more susceptible to sunlight-induced damage than MS2. This is consistent with UV-254 studies which have previously reported hNoV to be more susceptible to photodamage than MS2,[34] and previously reported infectivity assays for poliovirus, another ssRNA virus with a genome similar in length to hNoV, which has likewise been reported to be more susceptible to endogenous sunlight damage than MS2.[13] Results from our study align well with previous reports indicating that MS2 inactivation rates for filters with 50% longpass cutoffs of 320 nm or longer are similar to the dark condition,[57] indicating that UV-A wavelengths have limited impact on the photoinactivation of MS2 in water free of exogenous sensitizers. Contrastingly, hNoV degradation rate constants with 320 nm cut-off filters (typically considered the photobiological cutoff between UV-A/UV-B) determined in this study were significantly different from the dark condition, regardless of the assay method employed (Table 1). This suggests that longer UV wavelengths play a more prominent role in the endogenous photodamage of hNoV, compared to MS2. Other viruses, such as PRD1, have demonstrated significant photoinactivation upon exposure to longer UV wavelengths (i.e., xenon lamp with 335 or 345 nm longpass filters).[57] This suggests that hNoV may behave more like PRD1, displaying a greater susceptibility to solar inactivation at longer wavelengths compared to MS2.

**Mechanistic Insights.** The genome-wide damage extrapolation failed to successfully predict the loss of infectivity for MS2 under solar radiation, as evidenced by the large overestimation of $k$ values compared to the culture-based assay. Previously published MS2 results with UV-254 have shown that the genome-wide damage extrapolation with a single-hit inactivation assumption accurately predicts the results of an infectivity assay for MS2.[33,34] Although the single-hit model has been extensively validated with UV-254 genomic damage with several single-stranded RNA viruses,[33,34] our results indicate that this extrapolation is not appropriate for sunlight and perhaps other light sources with similar characteristics, i.e., longer wavelengths or polychromatic light source-based inactivation. A potential explanation for the failure of the genome-wide damage extrapolation to predict infectivity under solar radiation may be that the *single-hit* assumption is no longer valid under these conditions, i.e., one photon damage event is not always enough to inactivate the virus. These damage events could take the form of less lethal or temporary photoproducts that impede some part of the RT-qPCR reverse transcription or amplification processes, but alone cannot lead to the complete inactivation of the virus. These results indicate that genomic damage from sunlight exposure is at least partly chemically distinct from the photoproducts formed during UV-254 inactivation. It should be noted that if the genome-wide damage extrapolation produced an *underestimation* of the culture-based results, this could indicate that important nongenomic damage mechanisms are missed by RT-qPCR measurement. However, since our results indicate that the extrapolation *overestimates* the culture-based results, this indicates that it is incorrectly describing the extent or impact of genomic damage on MS2 infectivity.

These results underscore the mechanistic differences between inactivation with UV-254 compared to longer wavelength polychromatic light sources, such as natural and simulated sunlight. Although typically photoinactivation is thought to operate primarily via genomic damage, and even more narrowly through the formation of pyrimidine dimers,[39,55] past work has shown that a greater variety of deleterious reactions can occur. UV-C radiation is known to produce UU dimer products including cyclobutene pyrimidine dimers (CPD), pyrimidine pyrimidone photoadducts, and their Deware valence isomers,[55] while hydrates 6-hydroxy-5,6-dihydrocytidine and 6-hydroxy-5,6-dihydrouridine have long been known to be important photoproducts of cytosine and uridine.[54] Extending to longer wavelengths and polychromatic light sources, much less is known about the mechanism of damage or photoproduct formation. An investigation of photoproduct formation in coliphage R17 RNA under monochromatic 280 nm radiation indicated that uridine photohydrates were the major products formed, and that formation of cyclobutene-type pyrimidine dimers was comparatively insignificant.[56] Analysis of UV-C irradiated RNA segments identified several photochemical modifications using mass spectrometry, with some also impeding the RT enzyme; however, similar experiments performed with simulated sunlight did not detect significant modifications using RT-qPCR or mass spectrometry.[58] Very few studies have considered the formation of U and C hydrate photoproducts inside the viral capsid during inactivation with sunlight.

Considering the unique sequence of each amplicon may provide insight into the susceptibility of different bases, and adjacent base combinations, to solar photodamage. The variation in $k$ values between amplicons measured in this study was small for both hNoV and MS2. When the same MS2 amplicons used in this study, originally designed by Pecson et al.,[42] were tested under UV-254, a much larger variation in RT-qPCR signal loss was exhibited.[33] If pyrimidine dimers were the main photoproducts driving amplicon degradation, we would anticipate amplicons with higher contents of paired pyrimidines to exhibit larger $k$ values. For both MS2 and hNoV, there was no evidence that a greater number of adjacent pyrimidine bases caused an amplicon to be more susceptible to sunlight photodamage. For MS2, the relative degradation rate between amplicons did appear to be positively correlated with an increase in uracil content (Figure 3), a trend that was mirrored for both the 280 and 305 nm longpass filter conditions. However, since the overall variation in the uracil content of amplicons was low (less than 3% difference between the highest and lowest content), further study is required to confirm this trend.

The loss of RT-qPCR signal for hNoV amplicons was significantly faster than MS2 amplicons, implying that the rate of damage to the assayed regions of hNoV genomic material was higher than for the assayed regions of MS2. The statistically insignificant variation in degradation rate between individual amplicons from the same virus under the same spectral conditions (Figures S9−S12), coupled with the large fraction (nearly 30%) of the genome assayed, rules out variable sensitivities in the genomic regions assayed as an explanation for this result. It was initially hypothesized that this could be


https://doi.org/10.1021/acs.est.1c01575
Environ. Sci. Technol. 2021, 55, 8783−8792

due to the length of the hNoV amplicons: since each amplicon was designed to cover 8−9% of the genome, hNoV amplicons were ∼500 bp and MS2 amplicons were ∼300 bp. However, even when normalized by the number of bases, the degradation of hNoV amplicons was significantly faster than MS2 amplicons under the 280 and 320 nm spectral conditions. The larger RT-qPCR signal loss per nucleotide base for hNoV compared to MS2 combined with the small variation in $k$ values between amplicons indicates that the increased susceptibility of hNoV to genomic photodamage is dependent on something other than genome length and primary structure. Although both viruses have ssRNA genomes, they likely have different secondary structures that could affect their photoreactivity.[59] The integrity of the capsid could also impact the local environment of the nucleic acids, i.e., encapsidated or free in solution. A recent study of UV-254 photodamage to ssRNA viral genomes found that encapsidation had no impact on photoreactivity of the nucleic acids;[55] however, similar experiments under sunlight conditions have not been reported.

Capsid damage appeared to play a more significant role in hNoV inactivation, compared to MS2. ET-RT-qPCR results support the assertion that the hNoV capsid is more susceptible to damage by sunlight, compared to the MS2 capsid. Incorporation of an enzyme pretreatment had a relatively small impact on the $k$ values for MS2 compared to RT-qPCR alone, while enzyme treatment resulted in significantly larger rate constants for hNoV. Although photoinactivation mechanisms are primarily attributed to genomic damage, previous studies have reported that light can impact capsid integrity. Specifically, chemical modifications in MS2 capsid proteins after UV-C treatment[60] and a greater reduction of infectivity in adenovirus after exposure to polychromatic medium pressure UV lamps over monochromatic low pressure even though the extent of genetic damage is the same[61] have both been reported. Although damage to the capsid may play a role in the photoinactivation for both MS2 and hNoV, evidence from both the RT-qPCR and ET-qPCR results from this study indicate that hNoV is more susceptible to capsid damage from simulated sunlight.

**Practical Implications.** Overall, this work provides practical and mechanistic insight into the endogenous sunlight inactivation of both bacteriophage MS2 and hNoV GII, a health-relevant virus that is thought to account for most recreational waterborne illnesses. This is the first study to date to investigate the effect of sunlight on hNoV. Under full sunlight conditions (280 nm longpass filter), amplicon degradation $k$ values determined using RT-qPCR or ET-RT-qPCR are the same order of magnitude of, yet smaller than, culture-based inactivation rate constants for MS2. Thus, when culturing is not possible, $k$ values derived using molecular methods may yield reasonable, conservative approximations of RNA virus inactivation. Although unable to provide a complete description of virion damage, considering that no other value is available in the literature, molecular methods can provide for the interim more accurate inputs for fate and transport models, rather than assuming inactivation due to sunlight is negligible. With this in mind, we posit that the ET-RT-qPCR derived $k$ for hNoV of 5.6 $cm^2/kJ$ ($\lambda$ = 280−700 nm) is a reasonable estimate for the photoinactivation rate constant of hNoV in clear water. Since ET-qPCR does not consider genome-wide damage, it is understood to be a conservative estimate. Although conservative values can be useful for modeling environmental persistence, the conservative bias of the estimate may also be a limitation to its broader application. Considering the NREL AM1.5G reference spectrum,[53] typical for a clear spring day at a latitude of 40°N, the integrated solar energy from 280 to 700 nm would provide 520 $W/m^2$ of midday sunlight, corresponding to a time-based inactivation rate constant of 0.17 $min^{-1}$. Under these light conditions, it would take 40 min to achieve a 3-log inactivation of hNoV in shallow near-surface clear sensitizer-free water. For inactivation in a well-mixed water column, the fluence-based rate constant should be used and the fluence must be corrected for light screening. Considering that cloud cover tends to reduce the UV region of sunlight less than the total global irradiance,[62] and that hNoV was inactivated by wavelengths into the UV-A range, in some conditions a rate constant normalized by the total combined UV-B and UV-A doses (i.e., $k_{UV}$ where sunlight fluence is integrated from $\lambda$ = 280 to 390 nm) may be more appropriate. Based on the ET-RT-qPCR measurements from this study, $k_{UV}$ would be 67 $cm^2/kJ$ for hNoV. Considering both genomic damage and capsid damage, hNoV appears to be more susceptible to photodamage with sunlight compared to MS2. This indicates that under the conditions used in the study, i.e., clear, exogeneous sensitizer-free water, MS2 may be an appropriate conservative surrogate for hNoV inactivation. Since endogenous inactivation mechanisms can dominate under some environmental conditions, further studies that explore the effect of exogenous photosensitizers on the environmental persistence of hNoV will expand upon the practical significance of this work.

## ■ ASSOCIATED CONTENT

### Supporting Information

The Supporting Information is available free of charge at https://pubs.acs.org/doi/10.1021/acs.est.1c01575.

Experimental workflow (Figure S1); absorbance spectra of PBS (Figure S2); inactivation of MS2 in sterile PBS (Figure S3); gel products for hNoV candidate assays (Figure S4); gel products for all MS2 candidate assays (Figure S5); fraction base content (Figure S6); compiled standard curves (Figure S7); inactivation of MS2 under different illumination intensities (Figure S8); MS2 amplicon degradation (Figure S9); hNoV amplicon degradation (Figure S10); comparative rate of RT-qPCR signal loss for each MS2 amplicon (Figure S11); comparative rate of RT-qPCR signal loss for each hNoV amplicon (Figure S12); summary of candidate assays (Table S1); comparison of first-order rate law (Table S2); example calculations; and raw data for genome-wide extrapolation calculations is available through the Stanford data repository[63] (PDF)

## ■ AUTHOR INFORMATION

### Corresponding Author

**Alexandria B. Boehm** − *Department of Civil & Environmental Engineering, Stanford University, Stanford, California 94305, United States; Engineering Research Center (ERC) for Re-inventing the Nation's Urban Water Infrastructure (ReNUWIt), Stanford, California 94305, United States;* orcid.org/0000-0002-8162-5090; Phone: +650 724-9128; Email: aboehm@stanford.edu



https://doi.org/10.1021/acs.est.1c01575
Environ. Sci. Technol. 2021, 55, 8783−8792

## Authors

**Stephanie K. Loeb** − *Department of Civil & Environmental Engineering, Stanford University, Stanford, California 94305, United States; Engineering Research Center (ERC) for Reinventing the Nation's Urban Water Infrastructure (ReNUWIt), Stanford, California 94305, United States;* orcid.org/0000-0002-8666-518X

**Wiley C. Jennings** − *Department of Civil & Environmental Engineering, Stanford University, Stanford, California 94305, United States*

**Krista Rule Wigginton** − *Department of Civil & Environmental Engineering, University of Michigan, Ann Arbor, Michigan 48109, United States;* orcid.org/0000-0001-6665-5112

Complete contact information is available at: https://pubs.acs.org/10.1021/acs.est.1c01575


## Notes

The authors declare no competing financial interest.

## ■ ACKNOWLEDGMENTS

This work was supported by NSF CBET-1804169 and EEC-1028968.

## ■ REFERENCES


(1) Shuval, H. Estimating the global burden of thalassogenic diseases: human infectious diseases caused by wastewater pollution of the marine environment. *J. Water Health* **2003**, *1*, 53−64.

(2) Cabelli, V. J.; Defour, A. P.; McCabe, L. J.; Levin, M. A. Swimming-associated gastroenteritis and water quality. *Am. J. Epidemiol.* **1982**, *115*, 606−616.

(3) Viau, E. J.; Lee, D.; Boehm, A. B. Swimmer Risk of Gastrointestinal Illness from Exposure to Tropical Coastal Waters Impacted by Terrestrial Dry-Weather Runoff. *Environ. Sci. Technol.* **2011**, *45*, 7158−7165.

(4) Boehm, A. B.; Soller, J. A.; Shanks, O. C. Human-Associated Fecal Quantitative Polymerase Chain Reaction Measurements and Simulated Risk of Gastrointestinal Illness in Recreational Waters Contaminated with Raw Sewage. *Environ. Sci. Technol. Lett.* **2015**, *2*, 270−275.

(5) Wade, T. J.; Augustine, S. A. J.; Griffin, S. M.; Sams, E. A.; Oshima, K. H.; Egorov, A. I.; Simmons, K. J.; Eason, T. N.; Dufour, A. P. Asymptomatic norovirus infection associated with swimming at a tropical beach: A prospective cohort study. *PLoS One* **2018**, *13*, No. e0195056.

(6) Tong, H. I.; Connell, C.; Boehm, A. B.; Lu, Y. Effective detection of human noroviruses in Hawaiian waters using enhanced RT-PCR methods. *Water Res.* **2011**, *45*, 5837−5848.

(7) Wyn-Jones, A. P.; Carducci, A.; Cook, N.; D'Agostino, M.; Divizia, M.; Fleischer, J.; Gantzer, C.; Gawler, A.; Girones, R.; Höller, C.; de Roda Husman, A. M.; Kay, D.; Kozyra, I.; López-Pila, J.; Muscillo, M.; José Nascimento, M. S.; Papageorgiou, G.; Rutjes, S.; Sellwood, J.; Szewzyk, R.; Wyer, M. Surveillance of adenoviruses and noroviruses in European recreational waters. *Water Res.* **2011**, *45*, 1025−1038.

(8) Aw, T. G.; Gin, K. Y.-H.; Ean Oon, L. L.; Chen, E. X.; Woo, C. H. Prevalence and Genotypes of Human Noroviruses in Tropical Urban Surface Waters and Clinical Samples in Singapore. *Appl. Environ. Microbiol.* **2009**, *75*, 4984−4992.

(9) Gentry, J.; Vinjé, J.; Guadagnoli, D.; Lipp, E. K. Norovirus Distribution within an Estuarine Environment. *Appl. Environ. Microbiol.* **2009**, *75*, 5474−5480.

(10) DiCaprio, E. Recent advances in human norovirus detection and cultivation methods. *Curr. Opin. Food Sci.* **2017**, *14*, 93−97.

(11) Knight, A.; Li, D.; Uyttendaele, M.; Jaykus, L.-A. A critical review of methods for detecting human noroviruses and predicting their infectivity. *Crit. Rev. Microbiol.* **2013**, *39*, 295−309.

(12) Silverman, A. I.; Peterson, B. M.; Boehm, A. B.; McNeill, K.; Nelson, K. L. Sunlight Inactivation of Human Viruses and Bacteriophages in Coastal Waters Containing Natural Photosensitizers. *Environ. Sci. Technol.* **2013**, *47*, 1870−1878.

(13) Love, D. C.; Silverman, A.; Nelson, K. L. Human Virus and Bacteriophage Inactivation in Clear Water by Simulated Sunlight Compared to Bacteriophage Inactivation at a Southern California Beach. *Environ. Sci. Technol.* **2010**, *44*, 6965−6970.

(14) Bae, J.; Schwab, K. J. Evaluation of Murine Norovirus, Feline Calicivirus, Poliovirus, and MS2 as Surrogates for Human Norovirus in a Model of Viral Persistence in Surface Water and Groundwater. *Appl. Environ. Microbiol.* **2008**, *74*, 477.

(15) Flannery, J.; Rajko-Nenow, P.; Keaveney, S.; O'Flaherty, V.; Doré, W. Simulated sunlight inactivation of norovirus and FRNA bacteriophage in seawater. *J. Appl. Microbiol.* **2013**, *115*, 915−922.

(16) Charles, K. J.; Shore, J.; Sellwood, J.; Laverick, M.; Hart, A.; Pedley, S. Assessment of the stability of human viruses and coliphage in groundwater by PCR and infectivity methods. *J. Appl. Microbiol.* **2009**, *106*, 1827−1837.

(17) Liu, P.; Jaykus, L.-A.; Wong, E.; Moe, C. Persistence of Norwalk Virus, Male-Specific Coliphage, and *Escherichia coli* on Stainless Steel Coupons and in Phosphate-Buffered Saline. *J. Food Prot.* **2012**, *75*, 2151−2157.

(18) Mattioli, M. C.; Sassoubre, L. M.; Russell, T. L.; Boehm, A. B. Decay of sewage-sourced microbial source tracking markers and fecal indicator bacteria in marine waters. *Water Res.* **2017**, *108*, 106−114.

(19) Boehm, A. B.; Graham, K. E.; Jennings, W. C. Can We Swim Yet? Systematic Review, Meta-Analysis, and Risk Assessment of Aging Sewage in Surface Waters. *Environ. Sci. Technol.* **2018**, *52*, 9634−9645.

(20) Arthur, S. E.; Gibson, K. E. Environmental persistence of Tulane virus — a surrogate for human norovirus. *Can. J. Microbiol.* **2016**, *62*, 449−454.

(21) Kohn, T.; Nelson, K. L. Sunlight-Mediated Inactivation of MS2 Coliphage via Exogenous Singlet Oxygen Produced by Sensitizers in Natural Waters. *Environ. Sci. Technol.* **2007**, *41*, 192−197.

(22) Boehm, A. B.; Yamahara, K. M.; Love, D. C.; Peterson, B. M.; McNeill, K.; Nelson, K. L. Covariation and Photoinactivation of Traditional and Novel Indicator Organisms and Human Viruses at a Sewage-Impacted Marine Beach. *Environ. Sci. Technol.* **2009**, *43*, 8046−8052.

(23) Sinton, L. W.; Finlay, R. K.; Lynch, P. A. Sunlight Inactivation of Fecal Bacteriophages and Bacteria in Sewage-Polluted Seawater. *Appl. Environ. Microbiol.* **1999**, *65*, 3605−3613.

(24) Silverman, A. I.; Nelson, K. L. Modeling the Endogenous Sunlight Inactivation Rates of Laboratory Strain and Wastewater *E. coli* and Enterococci Using Biological Weighting Functions. *Environ. Sci. Technol.* **2016**, *50*, 12292−12301.

(25) Maraccini, P. A.; Wenk, J.; Boehm, A. B. Photoinactivation of Eight Health-Relevant Bacterial Species: Determining the Importance of the Exogenous Indirect Mechanism. *Environ. Sci. Technol.* **2016**, *50*, 5050−5059.

(26) Nelson, K. L.; Boehm, A. B.; Davies-Colley, R. J.; Dodd, M. C.; Kohn, T.; Linden, K. G.; Liu, Y.; Maraccini, P. A.; McNeill, K.; Mitch, W. A.; Nguyen, T. H.; Parker, K. M.; Rodriguez, R. A.; Sassoubre, L. M.; Silverman, A. I.; Wigginton, K. R.; Zepp, R. G. Sunlight-mediated inactivation of health-relevant microorganisms in water: a review of mechanisms and modeling approaches. *Environ. Sci.: Process. Impacts* **2018**, *20*, 1089−1122.

(27) Araud, E.; Shisler, J. L.; Nguyen, T. H. Inactivation Mechanisms of Human and Animal Rotaviruses by Solar UVA and Visible Light. *Environ. Sci. Technol.* **2018**, *52*, 5682−5690.

(28) Mattle, M. J.; Vione, D.; Kohn, T. Conceptual Model and Experimental Framework to Determine the Contributions of Direct and Indirect Photoreactions to the Solar Disinfection of MS2, phiX174, and Adenovirus. *Environ. Sci. Technol.* **2015**, *49*, 334−342.

(29) Zhang, X.; Lardizabal, A.; Silverman, A. I.; Vione, D.; Kohn, T.; Nguyen, T. H.; Guest, J. S. Global Sensitivity Analysis of Environmental, Water Quality, Photoreactivity, and Engineering Design Parameters in Sunlight Inactivation of Viruses. *Environ. Sci. Technol.* **2020**, *54*, 8401−8410.
(30) Seitz, S. R.; Leon, J. S.; Schwab, K. J.; Lyon, G. M.; Dowd, M.; McDaniels, M.; Abdulhafid, G.; Fernandez, M. L.; Lindesmith, L. C.; Baric, R. S.; Moe, C. L. Norovirus Infectivity in Humans and Persistence in Water. *Appl. Environ. Microbiol.* **2011**, *77*, 6884−6888.
(31) Karim, M. R.; Fout, G. S.; Johnson, C. H.; White, K. M.; Parshionikar, S. U. Propidium monoazide reverse transcriptase PCR and RT-qPCR for detecting infectious enterovirus and norovirus. *J. Virol. Methods* **2015**, *219*, 51−61.
(32) Rönnqvist, M.; Mikkelä, A.; Tuominen, P.; Salo, S.; Maunula, L. Ultraviolet Light Inactivation of Murine Norovirus and Human Norovirus GII: PCR May Overestimate the Persistence of Noroviruses Even When Combined with Pre-PCR Treatments. *Food Environ. Virol.* **2014**, *6*, 48−57.
(33) Pecson, B. M.; Ackermann, M.; Kohn, T. Framework for Using Quantitative PCR as a Nonculture Based Method To Estimate Virus Infectivity. *Environ. Sci. Technol.* **2011**, *45*, 2257−2263.
(34) Rockey, N.; Young, S.; Kohn, T.; Pecson, B.; Wobus, C. E.; Raskin, L.; Wigginton, K. R. UV Disinfection of Human Norovirus: Evaluating Infectivity Using a Genome-Wide PCR-Based Approach. *Environ. Sci. Technol.* **2020**, *54*, 2851−2858.
(35) Calgua, B.; Carratalà, A.; Guerrero-Latorre, L.; de Abreu Corrêa, A.; Kohn, T.; Sommer, R.; Girones, R. UVC Inactivation of dsDNA and ssRNA Viruses in Water: UV Fluences and a qPCR-Based Approach to Evaluate Decay on Viral Infectivity. *Food Environ. Virol.* **2014**, *6*, 260−268.
(36) Ayala-Torres, S.; Chen, Y.; Svoboda, T.; Rosenblatt, J.; Van Houten, B. Analysis of Gene-Specific DNA Damage and Repair Using Quantitative Polymerase Chain Reaction. *Methods* **2000**, *22*, 135−147.
(37) Deagle, B. E.; Eveson, J. P.; Jarman, S. N. Quantification of damage in DNA recovered from highly degraded samples − a case study on DNA in faeces. *Front. Zool.* **2006**, *3*, No. 11.
(38) Miller, R. L.; Plagemann, P. G. W. Effect of Ultraviolet Light on Mengovirus: Formation of Uracil Dimers, Instability and Degradation of Capsid, and Covalent Linkage of Protein to Viral RNA. *J. Virol.* **1974**, *13*, 729−739.
(39) Wurtmann, E. J.; Wolin, S. L. RNA under attack: Cellular handling of RNA damage. *Crit. Rev. Biochem. Mol.* **2009**, *44*, 34−49.
(40) Li, D.; Baert, L.; Xia, M.; Zhong, W.; Van Coillie, E.; Jiang, X.; Uyttendaele, M. Evaluation of methods measuring the capsid integrity and/or functions of noroviruses by heat inactivation. *J. Virol. Methods* **2012**, *181*, 1−5.
(41) Dunkin, N.; Weng, S.; Coulter, C. G.; Jacangelo, J. G.; Schwab, K. J. Reduction of Human Norovirus GI, GII, and Surrogates by Peracetic Acid and Monochloramine in Municipal Secondary Wastewater Effluent. *Environ. Sci. Technol.* **2017**, *51*, 11918−11927.
(42) Pecson, B. M.; Martin, L. V.; Kohn, T. Quantitative PCR for Determining the Infectivity of Bacteriophage MS2 upon Inactivation by Heat, UV-B Radiation, and Singlet Oxygen: Advantages and Limitations of an Enzymatic Treatment To Reduce False-Positive Results. *Appl. Environ. Microbiol.* **2009**, *75*, 5544.
(43) Wigginton, K. R.; Pecson, B. M.; Sigstam, T.; Bosshard, F.; Kohn, T. Virus Inactivation Mechanisms: Impact of Disinfectants on Virus Function and Structural Integrity. *Environ. Sci. Technol.* **2012**, *46*, 12069−12078.
(44) Hutson, A. M.; Atmar, R. L.; Estes, M. K. Norovirus disease: changing epidemiology and host susceptibility factors. *Trends Microbiol.* **2004**, *12*, 279−287.
(45) Agency, U. S. E. P. *Method 1602 Malespecific (F+) and Somatic Coliphage in Water by Single Agar Layer (SAL) Procedure*; DIANE Publishing, 2000.
(46) Ettayebi, K.; Crawford, S. E.; Murakami, K.; Broughman, J. R.; Karandikar, U.; Tenge, V. R.; Neill, F. H.; Blutt, S. E.; Zeng, X.-L.; Qu, L.; Kou, B.; Opekun, A. R.; Burrin, D.; Graham, D. Y.; Ramani, S.; Atmar, R. L.; Estes, M. K. Replication of human noroviruses in stem cell−derived human enteroids. *Science* **2016**, *353*, 1387.
(47) Dunkin, N.; Weng, S.; Jacangelo, J. G.; Schwab, K. J. Minimizing Bias in Virally Seeded Water Treatment Studies: Evaluation of Optimal Bacteriophage and Mammalian Virus Preparation Methodologies. *Food Environ. Virol.* **2017**, *9*, 473−486.
(48) BMS, N. S. R. R. L., *March 2020 Solar Calendar. In Golden, Colorado*, 2020.
(49) Topping, J. R.; Schnerr, H.; Haines, J.; Scott, M.; Carter, M. J.; Willcocks, M. M.; Bellamy, K.; Brown, D. W.; Gray, J. J.; Gallimore, C. I.; Knight, A. I. Temperature inactivation of Feline calicivirus vaccine strain FCV F-9 in comparison with human noroviruses using an RNA exposure assay and reverse transcribed quantitative real-time polymerase chain reaction—A novel method for predicting virus infectivity. *J. Virol. Methods* **2009**, *156*, 89−95.
(50) Qiagen AllPrep PowerViral DNA/RNA Kit Handbook. In *For the Isolation of Viral and Bacterial Total Nucleic Acids From Wastewater and Stool Samples, Qigen* 2018, *Vol. 04/2018*, pp 1 19.
(51) Dwight, Z.; Palais, R.; Wittwer, C. T. uMELT: prediction of high-resolution melting curves and dynamic melting profiles of PCR products in a rich web application. *Bioinformatics* **2011**, *27*, 1019−1020.
(52) Morgan, M. (2019). *BiocManager: Access the Bioconductor Project Package Repository. R package version 1.30.10*. https://CRAN.R-project.org/package=BiocManager.
(53) ASTM, American Society for Testing and Materials (ASTM) Terrestrial Reference Spectra for Photovoltaic Performance Evaluation. In ASTM G173-03 ed.; (ASTM), A. S. f. T. a. M., Ed. 1999.
(54) Miller, N.; Cerutti, P. Structure of the photohydration products of cytidine and uridine. *Proc. Natl. Acad. Sci. U.S.A.* **1968**, *59*, 34−38.
(55) Qiao, Z.; Ye, Y.; Chang, P. H.; Thirunarayanan, D.; Wigginton, K. R. Nucleic Acid Photolysis by UV254 and the Impact of Virus Encapsidation. *Environ. Sci. Technol.* **2018**, *52*, 10408−10415.
(56) Remsen, J. F.; Miller, N.; Cerutti, P. A. Photohydration of Uridine in the RNA of Coliphage R17, II. The Relationship between Ultraviolet Inactivation and Uridine Photohydration. *Proc. Natl. Acad. Sci. U.S.A.* **1970**, *65*, 460−466.
(57) Fisher, M. B.; Love, D. C.; Schuech, R.; Nelson, K. L. Simulated Sunlight Action Spectra for Inactivation of MS2 and PRD1 Bacteriophages in Clear Water. *Environ. Sci. Technol.* **2011**, *45*, 9249−9255.
(58) Qiao, Z.; Wigginton, K. R. Direct and Indirect Photochemical Reactions in Viral RNA Measured with RT-qPCR and Mass Spectrometry. *Environ. Sci. Technol.* **2016**, *50*, 13371−13379.
(59) Pearson, M.; Johns, H. E. Suppression of hydrate and dimer formation in ultraviolet-irradiated poly (A + U) relative to poly U. *J. Mol. Biol.* **1966**, *20*, 215−229.
(60) Rule Wigginton, K.; Menin, L.; Montoya, J. P.; Kohn, T. Oxidation of Virus Proteins during UV254 and Singlet Oxygen Mediated Inactivation. *Environ. Sci. Technol.* **2010**, *44*, 5437−5443.
(61) Eischeid, A. C.; Meyer, J. N.; Linden, K. G. UV Disinfection of Adenoviruses: Molecular Indications of DNA Damage Efficiency. *Appl. Environ. Microbiol.* **2009**, *75*, 23.
(62) Calbó, J.; Pagès, D.; González, J.-A. Empirical studies of cloud effects on UV radiation: A review. *Rev. Geophys.* **2005**, *43*, 1−28.
(63) Loeb, S. K.; Boehm, A. B. Data on persistence of human norovirus and MS2 in water with sunlight exposure. Stanford Digital Repository, 2021, Available at: https://purl.stanford.edu/dr150yk2588.


https://doi.org/10.1021/acs.est.1c01575
*Environ. Sci. Technol.* 2021, 55, 8783−8792